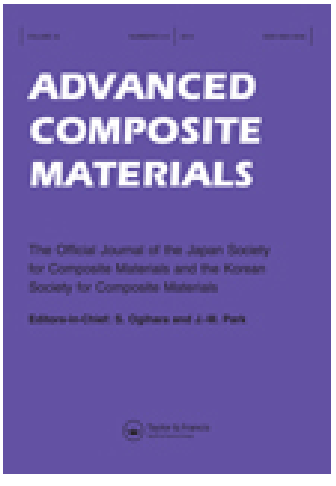

Advanced Composite Materials
Publication details, including instructions for authors and subscription information:
http://www.tandfonline.com/loi/tacm20

Impact damage monitoring of FRP pressure vessels based on impact force identification

Satoshi Atobe[a], Sunao Sugimoto[b], Ning Hu[c] & Hisao Fukunaga[a]

[a] Department of Aerospace Engineering, Tohoku University, 6-6-01 Aramaki-aza-Aoba, Aoba-ku, Sendai 980-8579, Japan

[b] Aerospace Research and Development Directorate, Japan Aerospace Exploration Agency, 6-13-1 Ohosawa, Mitaka, Tokyo 181-0015, Japan

[c] Department of Mechanical Engineering, Chiba University, 1-33 Yayoi-cho, Inage-ku, Chiba 263-8522, Japan

Published online: 14 May 2014.

To cite this article: Satoshi Atobe, Sunao Sugimoto, Ning Hu & Hisao Fukunaga (2014) Impact damage monitoring of FRP pressure vessels based on impact force identification, Advanced Composite Materials, 23:5-6, 491-505, DOI: 10.1080/09243046.2014.915112

To link to this article: http://dx.doi.org/10.1080/09243046.2014.915112

Advanced Composite Materials, 2014
Vol. 23, Nos. 5–6, 491–505, http://dx.doi.org/10.1080/09243046.2014.915112

Impact damage monitoring of FRP pressure vessels based on impact force identification

Satoshi Atobe[a]*, Sunao Sugimoto[b], Ning Hu[c] and Hisao Fukunaga[a]

[a]*Department of Aerospace Engineering, Tohoku University, 6-6-01 Aramaki-aza-Aoba, Aoba-ku, Sendai 980-8579, Japan;* [b]*Aerospace Research and Development Directorate, Japan Aerospace Exploration Agency, 6-13-1 Ohosawa, Mitaka, Tokyo 181-0015, Japan;* [c]*Department of Mechanical Engineering, Chiba University, 1-33 Yayoi-cho, Inage-ku, Chiba 263-8522, Japan*

(*Received 5 February 2014; accepted 10 April 2014*)

In this paper, a method for monitoring impact damage of FRP pressure vessels is discussed. To estimate the location and extent of the impact damage, strains are measured at several locations on the surface of the structure, and impact force identification is performed using those data so as to obtain information on the impact which caused the damage. The location and force history of the impact are identified using an identification method based on experimental transfer matrices which relate the impact force to the corresponding strain responses. Here, experimental transfer matrices are determined from the measured data acquired by impact tests that do not wreak impact damages. The location of the impact damage is predicted from the identified impact location. As to the extent of the impact damage, the peak value and the duration of the identified force history are used to estimate the damage initiation and the damage size, respectively. In order to examine the validity of the method, monitoring of impact damages induced by drop-weight impact tests is demonstrated.

Keywords: impact damage; FRP pressure vessel; impact location; force history; identification; structural health monitoring

1. Introduction

One of the concerns in using composite structures is the degradation of structural stiffness that occurs when impact damages are induced by foreign object impacts.[1] For aerospace structures, impacts by birds, hail, and tools are some of the threats. In the past few decades, development of structural health monitoring (SHM) techniques for composite materials has been carried out by many researchers in order to extend the application of composite structures.[2] A SHM system is designed to ensure the safety of composite structures automatically and in real time by monitoring the damage and assessing the structural integrity using the data acquired from a built-in sensor network. In the case of impact damage monitoring, various types of SHM techniques have been reported thus far. For example, methods for monitoring impact damages based on the signals from optical fiber sensors have been studied extensively.[3–8] There are also SHM techniques [9,10] which use the change in electric resistance of the composite structure that occurs before and after the impact damage.

*Corresponding author. Email: atobe@ssl.mech.tohoku.ac.jp

Impact force identification is also an effective way to obtain useful information for predicting the location and extent of the impact-induced damage. Sung et al. [11] have reported the method to monitor the damage by using a neural network to identify the impact location from the differences in the arrival times of the acoustic waves to the PZT sensors, and wavelet transform of the acoustic emission wave for estimating the qualitative severity of the damage. A technique similar to that reported in [11] was developed by Jang et al. [12] using fiber Bragg grating sensors, and its effectiveness was verified experimentally with composite flat and stiffened panels. Hu et al. [13] and Fukunaga et al. [14] proposed a convenient method which monitors the damage of CFRP structures by identifying the location and force history of the applied impact from measured strain data using transfer matrices that relate the impact force to the corresponding sensor responses. In their study, drop-weight impact tests of CFRP laminated plates were conducted, and the change in force history due to the impact-induced damage was focused. When impact damages were not induced within the laminated plates, the force history was similar to a sine pulse. On the other hand, when impact damages were induced, the force dropped at the time of damage initiation, and after that the force history fluctuated as the damage grew. Thus, it was concluded that, if the induced damage is not severe, the initiation of damage can be easily judged by examining the identified force history. In a subsequent paper,[15] the peak value of the identified force was used to quantitatively assess the extent of the damage. The results from the previous studies signify that impact damage monitoring based on impact force identification is an effective approach, but further investigations must be conducted to improve it.

The present paper deals with impact damage monitoring of FRP pressure vessels. In the introduced method, the location and force history of the impact are identified from the strain responses measured at several locations of the structure first, and then the extent of the impact damage are estimated from the identified force. Here, the peak value and the duration of the identified force are adopted as the parameters for estimating the extent of damage. The impact force is identified by employing the identification method based on experimental transfer matrices.[14,15] In order to demonstrate the validity of the present method, drop-weight impact tests are conducted and the damages induced during the tests are monitored.

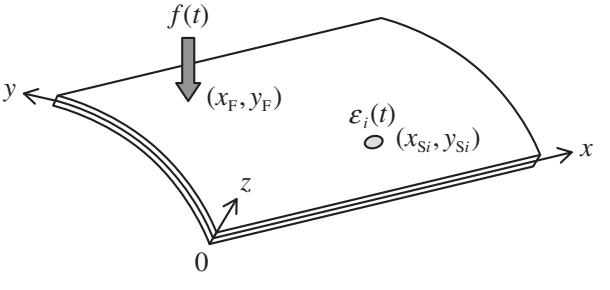

Figure 1. Composite pressure vessel subjected to impact force.

2. Method for identifying the location and force history of an impact acting on a composite pressure vessel

2.1. Construction of experimental transfer matrices

Figure 1 depicts a composite pressure vessel subjected to an impact force. In this study, a coordinate system (x, y, z) shown in Figure 1 is adopted, whose x, y, and z axes coincide with the longitudinal, circumferential, and radial directions, respectively. The impact force acts vertically on the outer surface of the pressure vessel at (x_F, y_F), and a compressive force $f(t)$ is assumed. The corresponding strain responses $\varepsilon_i(t)$ $(i = 1, \ldots, M)$ are measured at a total of M $(\geqslant 3)$ locations (x_{Si}, y_{Si}) $(i = 1, \ldots, M)$ on the outer surface of the specimen by using biaxial strain gauges. The relation between the impact force and the response of the i th sensor can be expressed in the following equation:

$$\boldsymbol{\varepsilon}_i = \mathbf{G}(x_F, y_F, x_{Si}, y_{Si})\, \boldsymbol{f} \tag{1}$$

where

$$\boldsymbol{\varepsilon}_i = [\ \varepsilon_i(t_1)\ \varepsilon_i(t_2) \cdots \varepsilon_i(t_N)\ ]^T, \qquad \boldsymbol{f} = [\ f(t_1)\, f(t_2) \cdots f(t_N)\ ]^T,$$

$$\mathbf{G}(x_F, y_F, x_{Si}, y_{Si}) = \begin{bmatrix} g_{i,1} & 0 & \cdots & 0 \\ g_{i,2} & g_{i,1} & \ddots & \vdots \\ \vdots & \vdots & \ddots & 0 \\ g_{i,N} & g_{i,N-1} & \cdots & g_{i,1} \end{bmatrix}. \tag{2}$$

Here, $\varepsilon_i(t_n)$ and $f(t_n)$ are the strain and force measured at the time $t_n = n\ \Delta t_s$ $(n = 1, \ldots, N)$, respectively. $\mathbf{G}(x_F, y_F, x_{Si}, y_{Si})$ is a transfer matrix composed of the Green's function. It is worthwhile to note that the transfer matrix is defined by a function of the impact location (x_F, y_F) and sensor location (x_{Si}, y_{Si}), and is not dependent on the force history.

By rewriting Equation (1), we obtain

$$\boldsymbol{\varepsilon}_i = \mathbf{F}\ \boldsymbol{g}_i \tag{3}$$

where

$$\boldsymbol{g}_i = [g_{i,1}\, g_{i,2} \cdots g_{i,N}\ ]^T, \quad \mathbf{F} = \begin{bmatrix} f(t_1) & 0 & \cdots & 0 \\ f(t_2) & f(t_1) & \ddots & \vdots \\ \vdots & \vdots & \ddots & 0 \\ f(t_N) & f(t_{N-1}) & \cdots & f(t_1) \end{bmatrix}. \tag{4}$$

The transfer matrix is constructed experimentally by conducting impact tests with an impulse hammer. The specimen must be struck with care so that impact damage is not induced during these impact tests. The components of the transfer matrix are determined in a way where the estimated strains given by Equation (3) using the measured force histories, are adjusted to match the measured strains as much as possible. In order to construct a reliable transfer matrix, the experimental data to use are acquired by

repeating the impact tests K times. Thus, the components of the transfer matrix are obtained by solving the minimization problem as follows:

$$\begin{aligned} &\text{minimize}: \sum_{k=1}^{K} \| \boldsymbol{\varepsilon}_i^k - \mathbf{F}^k \boldsymbol{g}_i \|^2 \\ &\text{variables}: \boldsymbol{g}_i \end{aligned} \tag{5}$$

where $\boldsymbol{\varepsilon}_i^k$ and $\mathbf{F}^k$ are the vector of measured strains and the force matrix of the k th impact test, respectively. Here, the least-squares method is used to solve Equation (5).

As previously noted, the transfer matrix is defined by a function of the impact location $(x_{\mathrm{F}}, y_{\mathrm{F}})$ and sensor location $(x_{\mathrm{S}i}, y_{\mathrm{S}i})$. Therefore, to identify an impact force acting at an unknown location using the measured strains obtained from multiple sensors, the transfer matrix is required for each sensor and for an arbitrary $(x_{\mathrm{F}}, y_{\mathrm{F}})$. Thus, the whole identification region is divided into some discrete grid areas, as shown in Figure 2(a), and the impact tests are conducted at every grid node. Then, by employing Equation (5), the experimental transfer matrices are constructed for each set relating one node (impact location) to one sensor location. For an impact location inside the four nodes of each grid area, the transfer matrix is obtained by an interpolation operation using shape functions similar to those used in finite element analyses. When the shape functions of a four-node two-dimensional element are used, as depicted in Figure 2(b), the interpolation of transfer matrix is expressed as:

$$\mathbf{G}(x_{\mathrm{F}}, y_{\mathrm{F}}, x_{\mathrm{S}i}, y_{\mathrm{S}i}) = \sum_{l=1}^{4} N_l \, \mathbf{G}(x_l, y_l, x_{\mathrm{S}i}, y_{\mathrm{S}i}) \tag{6}$$

where

$$\begin{aligned} N_1 &= \frac{1}{4}(1-\xi_{\mathrm{F}})(1-\eta_{\mathrm{F}}), \quad N_2 = \frac{1}{4}(1+\xi_{\mathrm{F}})(1-\eta_{\mathrm{F}}), \\ N_3 &= \frac{1}{4}(1+\xi_{\mathrm{F}})(1+\eta_{\mathrm{F}}), \quad N_4 = \frac{1}{4}(1-\xi_{\mathrm{F}})(1+\eta_{\mathrm{F}}). \end{aligned} \tag{7}$$

Here, (x_l, y_l) are the coordinates of node l, and $(\xi_{\mathrm{F}}, \eta_{\mathrm{F}})$ is the local coordinates of the impact location.

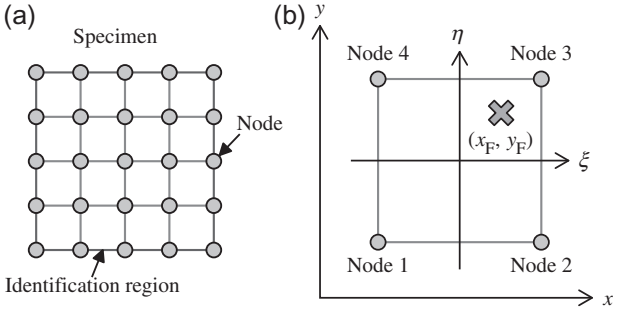

Figure 2. Construction of experimental transfer matrices. (a) Grid nodes (b) Interpolation.

2.2. Method for identifying the impact force

In this study, the location and force history of the impact are identified by an iterative method that uses the preliminarily constructed experimental transfer matrices. The identification procedure is described in Figure 3.

When the impact location is determined, the force history is identified by minimizing the deviation between the measured strains and the strains estimated from Equation (1) using the experimental transfer matrices. Then, the identification problem can be expressed as

$$\begin{aligned} &\text{minimize} : \sum_{i=1}^{M} \| \boldsymbol{\varepsilon}_i - \mathbf{G}(x_{\mathrm{F}}, y_{\mathrm{F}}, x_{\mathrm{S}i}, y_{\mathrm{S}i})\, \boldsymbol{f} \|^2 \\ &\text{subject to} : f(t) \geqslant 0 \\ &\text{variables} : \boldsymbol{f} \end{aligned} \tag{8}$$

Here, the quadratic programming method is used to solve Equation (8).

First, the impact location is approximated by conducting force history identification at every grid node where the experimental transfer matrices were constructed. The location of the node at which the objective function of Equation (8) becomes the minimum is chosen as the initial coordinates of the estimated impact location $(x_{\mathrm{e}}, y_{\mathrm{e}})$.

When the impact location is approximated as $(x_{\mathrm{e}}, y_{\mathrm{e}})$, the estimated force history $\boldsymbol{f}_{\mathrm{e}}$ is calculated at the location by employing Equation (8). Then, the accurate impact location which minimizes the deviation between the measured strains and the strains calculated from the estimated force history is obtained from the following minimization problem.

$$\begin{aligned} &\text{minimize} : \sum_{i=1}^{M} \| \boldsymbol{\varepsilon}_i - \mathbf{G}(x_{\mathrm{F}}, y_{\mathrm{F}}, x_{\mathrm{S}i}, y_{\mathrm{S}i})\, \boldsymbol{f}_{\mathrm{e}} \|^2 \\ &\text{variables} : x_{\mathrm{F}}, y_{\mathrm{F}} \end{aligned} \tag{9}$$

Here, Equation (9) is solved using the conjugate gradient method with the golden section search method. The estimated impact location is updated with the location obtained from Equation (9), and the same process is repeated until the impact location converges to a certain point.

Lastly, force history identification is performed at the identified impact location.

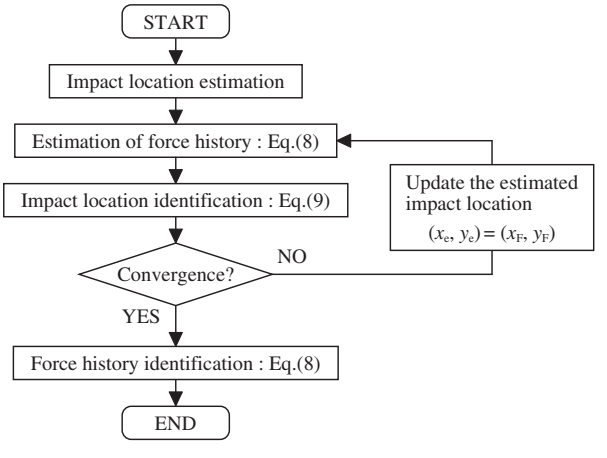

Figure 3. Flow chart of impact force identification.

3. Impact tests

Figure 4 shows the FRP pressure vessel (Toray Industries SÉCURE CF TC8515) used in this study. An empty vessel is placed on a cradle and fixed by two steel wires. The length, outer diameter, and thickness of the pressure vessel are 473 mm, 173.5 mm, and 5.5 mm, respectively. As shown in Figure 5, the pressure vessel consists of an aluminum liner, a carbon FRP layer, a glass FRP layer, and a resin layer.

The schematic of the experimental setup is shown in Figure 6. Instruments used to apply the impact forces are an impulse hammer (Dytran Instruments 5850B) and a drop-weight impact tester (Instron Dynatup 9250HV). The impulse hammer is used for the construction of the experimental transfer matrices, while the drop-weight impact tester is used in the experiments for impact damage monitoring. Four biaxial strain gauges are bonded on the outer surface of the vessel, and the strain responses are recorded along with the force history by a data acquisition system (Keyence NR-500). The sampling time is set as $\Delta t_s = 20\ \mu$s. A computer is used to identify the impact force from the measured data, and to estimate the impact damage from the identified force.

As shown in Figure 4, the identification region of the impact force is 80 mm square. The identification region is equally divided into four sections in the directions of the x and y axes, which means that the experimental transfer matrices are constructed at 25 grid nodes. The number of impact tests conducted at each node for the construction of the experimental transfer matrix is $K = 5$.

The details of the impact tests conducted for impact damage monitoring are summarized in Table 1. In the table, the coordinates of the impact locations are indicated in millimeters, and the origin of the coordinate system is placed at the center of the identification region as depicted in Figure 4.

Examples of force histories and the corresponding strain responses are shown in Figure 7. Figure 7(a) is the data measured for constructing the experimental transfer matrix at the center grid node, while Figures 7(b) and (c) correspond to Cases B and L in Table 1, respectively. In the present study, an impact tip made of hard plastic was attached to the impulse hammer, and a 0.625-inch diameter hemispherical tup insert made of steel was attached to the drop-weight impact tester. As can be seen from Figures 7(a) and (b), the peak and duration of the force differ between the impulse hammer and the drop-weight impact tester. Moreover, when the impact energy is large enough to induce impact damage, such as the case of Figure 7(c), a sharp drop and some fluctuations can be seen in the force history.

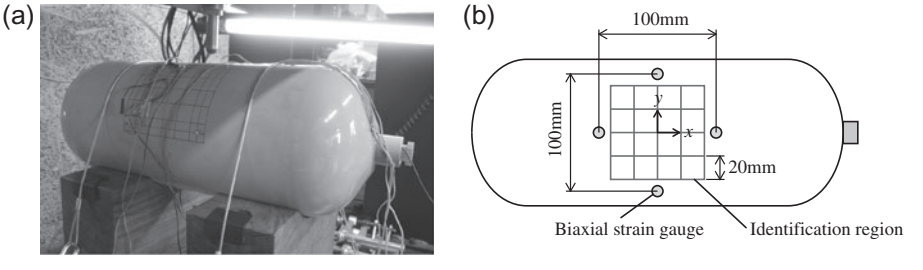

Figure 4. FRP pressure vessel.

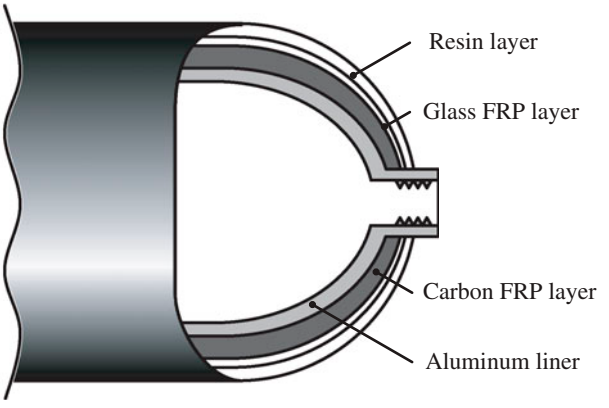

Figure 5. Cutaway of FRP pressure vessel.

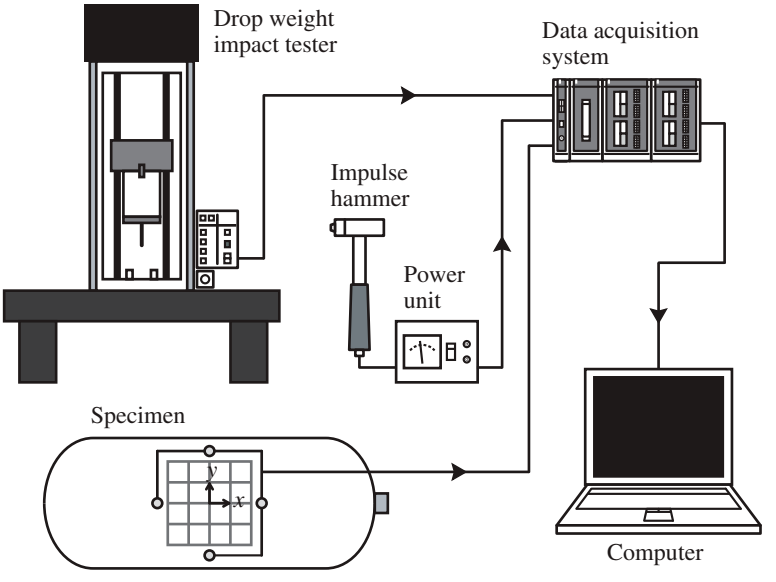

Figure 6. Experimental setup.

The extent of impact damage was inspected after the impact tests with a thermographic NDT system (Thermal Wave Imaging EchoTherm). Figure 8 shows the thermal image taken after the impact test for Case N in Table 1. The shaded area was considered as the impact damage, and the size was measured by counting the number of pixels of the shaded area.

4. Results and discussion

4.1. Impact force identification

The identification results of impact location for the cases in which impact damage was not induced, i.e. Cases A to J, are shown in Figure 9. In the figure, the marks

Table 1. Details of the tests conducted for impact damage monitoring.

	Impact energy (J)	Impact location (x_F, y_F) in mm	Peak force F_{peak} (kN)	Impact damage (mm^2)
Case A	1	(−3, 27)	2.33	0
Case B	1	(3, −8)	2.51	0
Case C	1	(2, 18)	2.48	0
Case D	2	(−16, 25)	3.89	0
Case E	2	(17, −25)	3.69	0
Case F	2	(−18, −21)	3.79	0
Case G	2	(−5, −10)	3.45	0
Case H	3	(−13, 5)	4.38	0
Case I	3	(13, 10)	4.25	0
Case J	4	(18, 25)	4.77	0
Case K	7	(−13, 5)	4.92	564
Case L	7	(3, −8)	4.60	173
Case M	9	(−3, 27)	4.85	890
Case N	9	(−5, −10)	4.76	817
Case O	9	(13, 10)	4.97	357
Case P	11	(−16, 25)	5.31	589
Case Q	13	(−18, −21)	5.45	1314

◎ and ⊠ denote the identified location and the measured location, respectively. The coordinates of the identified locations and their errors are indicated in Table 2. In order to examine the accuracy of impact location identification, the distance between the identified location and the measured location will be defined as the identification error. For the 10 non-damaged cases, the maximum error and the average error of the identified locations were 11.6 and 5.6 mm, respectively. Figure 10 shows the identification result of force history for Case E, whose error of the identified location was 8.0 mm. In this figure, the dashed and solid lines denote the identified force and the measured force, respectively, and the mark ◦ denotes the peak value of each force. As can be seen from the figure, identified force overestimates the force a little, but it is in good agreement with the measured one. The peak value of the identified force was 9.3% larger than that of the measured force. As to the maximum and average errors of the peak force for the 10 non-damaged cases, they were 27.0 and 19.9%, respectively.

Figure 11 shows the identification results of the impact location for Cases K to Q, in which the impact damage was induced. Refer to Table 2 for the coordinates of the identified locations and their errors. The impact locations were identified within the error of 7.6 mm. The results reveal that there is no large difference in the accuracy of the identified impact locations between the damaged cases and the non-damaged cases. Figure 12 shows the result of force history identification for Case N. Although the error of the identified location was only 2.3 mm, the deviation between the identified force and the measured force is rather large, compared to the non-damaged case shown in Figure 10. A similarity in the shape of the force history can be seen, but the magnitude is remarkably overestimated. The identified peak force was 53.1% larger than the measured peak force in this case. This deviation is caused by the degradation of the stiffness due to the induced impact damage. In the present impact force identification, the influence of the degradation of the local stiffness at the impact point is neglected in the construction of the transfer matrices.

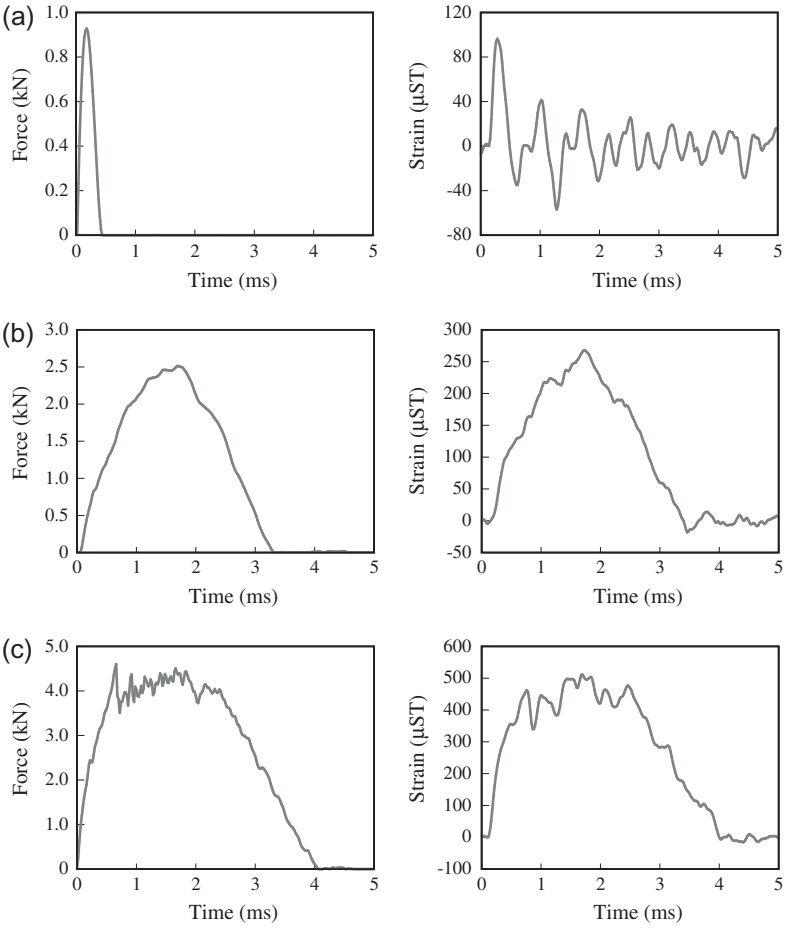

Figure 7. Force history of the impact and the corresponding strain response. (a) Impulse hammer (b) Drop-weight impact tester ($E = 1$ J) (c) Drop-weight impact tester ($E = 7$ J).

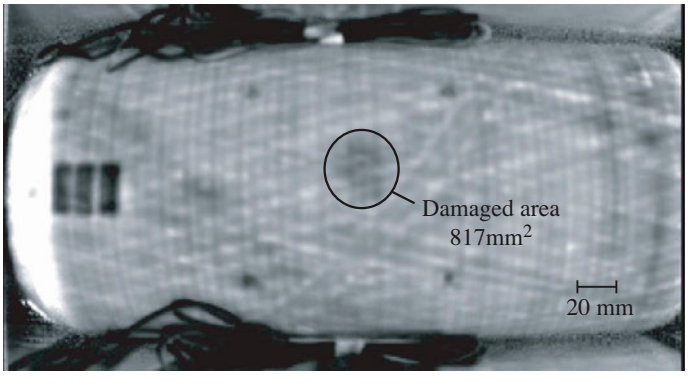

Figure 8. Thermographic NDT of the impacted FRP pressure vessel (Case N).

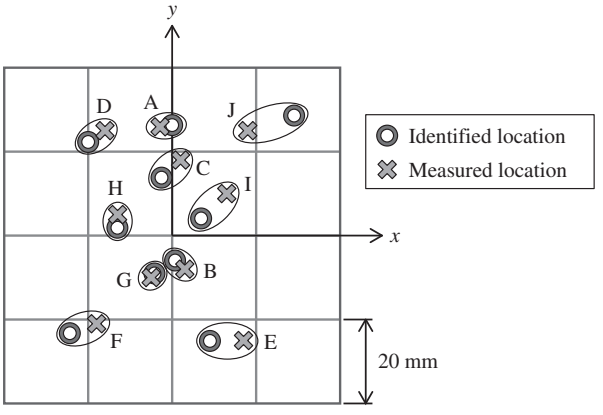

Figure 9. Identification results of the impact location for the cases in which impact damage was not induced.

4.2. *Impact damage monitoring*

The location of the impact damage can be predicted with ease, owing to the high accuracy of the identified impact location. In order to estimate the extent of the impact damage from the identified force, a relationship between the impact force and the induced damage is essential.

First, the validity of using the peak value of the identified force for the estimation of the impact damage will be examined. Figure 13 shows the correlation between the measured peak force F_{peak} and the size of the induced impact damage. Let us note that, to obtain the data shown in Figure 13, several more impact tests were conducted besides the tests indicated in Table 1. In the figure, the dashed line shows the linear least squares fit line determined using the measured peak forces of the damaged cases. As can be seen from the figure, impact damage is induced when the peak force is larger than a threshold value ($= 4.2$ kN), and the size of the damage increases as the peak force increases. Figure 14 shows the correlation between the impact energy E and the peak force F_{peak}. In the figure, the marks ◇ and ○ denote the peak value of the identified force and that of the measured force, respectively. The solid and dashed lines denote the linear least squares fit lines determined using the measured data obtained from the impact tests of the non-damaged specimens and the damaged specimens, respectively. The figure reveals that the peak value of the identified force is linearly related to the square root of the impact energy, which is similar to the following relationship obtained from a SDOF spring-mass model [16] that assumes linear elastic response:

$$F_{\text{peak}} = \sqrt{2K_{\text{s}}E} \tag{10}$$

where K_{s} represents the structural stiffness of an intact structure. In the case of the measured force, the slope of the peak force changes at the point of 4.2 kN where the impact force starts to induce damage and degrade the structural stiffness. As mentioned before, the identified force tends to overestimate the actual force when damage is induced by the impact, because the influence of stiffness degradation is neglected in the impact force identification based on experimental transfer matrices. Therefore, when the threshold value for damage initiation is determined experimentally, the peak value

Table 2. Results of impact force identification.

	Impact location (x_F, y_F) in mm	Identified location (x_{ID}, y_{ID}) in mm	Error (mm)	Peak force F_{peak} (kN)	Identified F_{peak} (kN)	Error (%)
Case A	(−3, 27)	(0.0, 26.3)	3.1	2.33	2.70	15.9
Case B	(3, −8)	(0.7, −5.9)	3.1	2.51	3.19	27.0
Case C	(2, 18)	(−2.5, 13.8)	6.2	2.48	2.88	16.4
Case D	(−16, 25)	(−20.0, 22.3)	4.8	3.89	4.53	16.6
Case E	(17, −25)	(9.0, −25.1)	8.0	3.69	4.03	9.3
Case F	(−18, −21)	(−24.4, −23.3)	6.8	3.79	4.53	19.5
Case G	(−5, −10)	(−4.2, −9.0)	1.3	3.45	4.32	25.2
Case H	(−13, 5)	(−13.0, 1.9)	3.1	4.38	5.27	20.3
Case I	(13, 10)	(6.9, 4.1)	8.5	4.25	5.18	21.9
Case J	(18, 25)	(29.0, 28.6)	11.6	4.77	6.06	27.0
Case K	(−13, 5)	(−9.5, 0.0)	6.1	4.92	6.33	28.8
Case L	(3, −8)	(0.7, −3.1)	5.4	4.60	6.48	40.7
Case M	(−3, 27)	(0.0, 31.7)	5.6	4.85	7.27	49.9
Case N	(−5, −10)	(−2.9, −9.2)	2.3	4.76	7.29	53.1
Case O	(13, 10)	(9.2, 6.2)	5.4	4.97	7.22	45.2
Case P	(−16, 25)	(−14.4, 21.5)	3.9	5.31	6.97	31.3
Case Q	(−18, −21)	(−25.3, −22.8)	7.6	5.45	8.40	54.1

of the identified force could be used to judge whether the structure is damaged or not. On the other hand, it may be difficult to quantitatively assess the size of the impact damage from the identified peak force.

Next, the duration of the force will be discussed. The correlation between the duration and the size of the induced impact damage is shown in Figure 15. The dashed line in the figure shows the linear least squares fit line determined using the duration of the measured forces for the damaged cases. As in the case of the peak force, impact damage is induced when the duration is longer than a certain length (=3.53 ms), and the size of the damage increases in proportion to the duration. Figure 16 shows the correlation between the impact energy and the duration. In the figure, the linear least squares fit line determined using the measured data obtained from the impact tests of

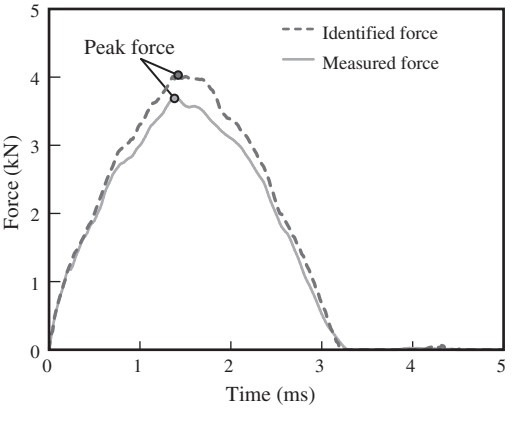

Figure 10. Identification result of the force history for Case E ($E = 2$ J).

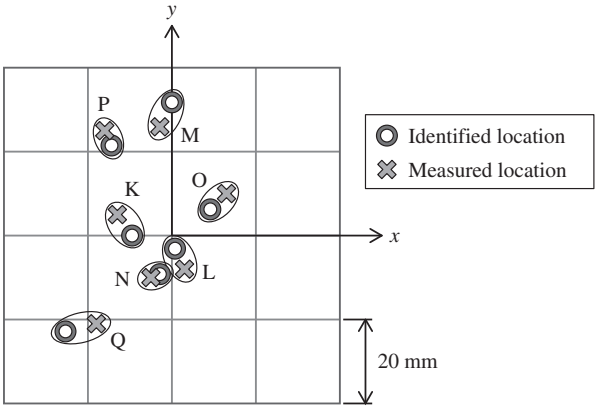

Figure 11. Identification results of the impact location for the cases in which impact damage was induced.

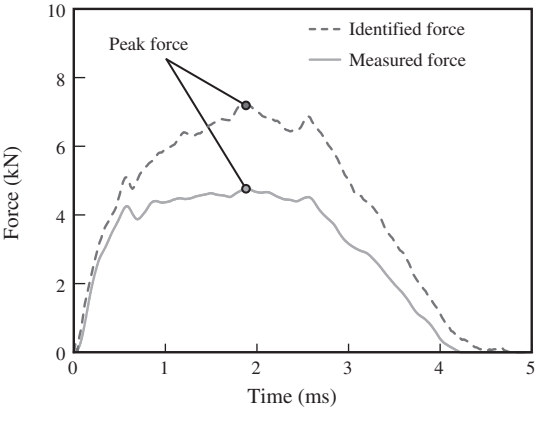

Figure 12. Identification result of the force history for Case N ($E = 9$ J).

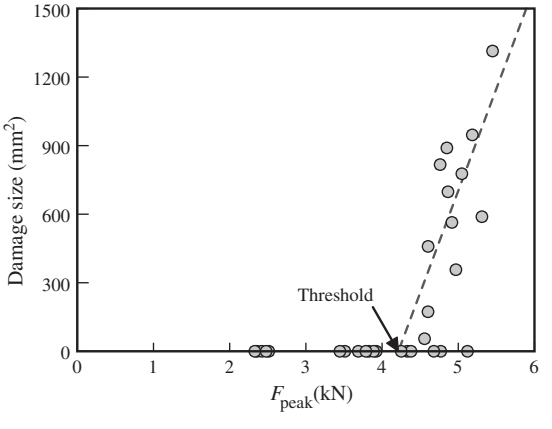

Figure 13. Correlation between the peak force and the size of impact damage.

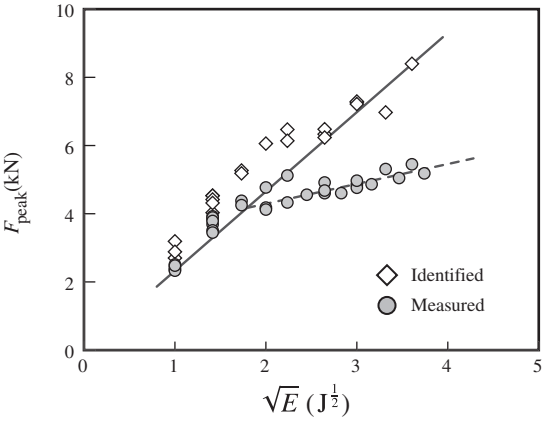

Figure 14. Correlation between the impact energy and the peak force.

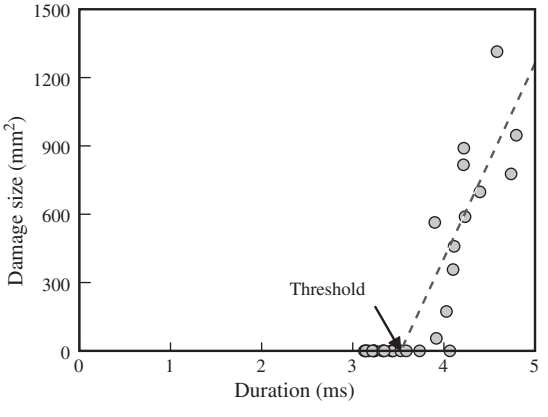

Figure 15. Correlation between the duration of impact force and the size of impact damage.

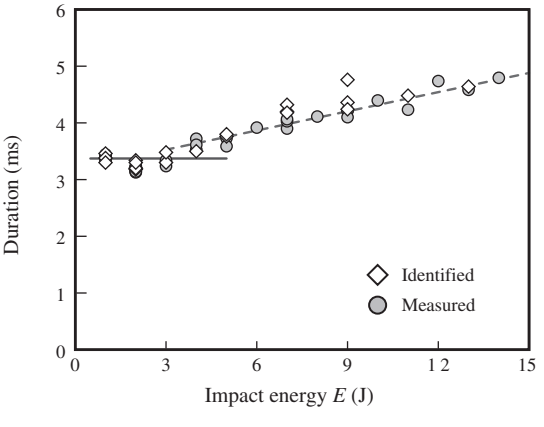

Figure 16. Correlation between the impact energy and the duration of impact force.

the non-damaged specimens and the line for the damaged specimens are shown by a solid line and a dashed line, respectively. When the impact energy is small, the duration does not vary with the impact energy. This fact corresponds to the duration determined from the aforementioned SDOF spring-mass model, $T_c = \pi\sqrt{M_i/K_s}$, where M_i is the impactor mass. As the impact energy increases and damage is induced, the duration becomes longer. In contrast to the peak force, the duration of the identified force agrees well with that of the measured force, as shown in Figure 16. The maximum error between the duration of the identified force and the duration measured was 12.9%. Thus, by referring to a relation like Figure 15 that is predetermined experimentally, the damage size could be estimated more accurately from the identified duration rather than the identified peak force.

In this paper, small size of damages such as barely visible impact damages is considered due to the low-velocity impacts by foreign objects which are stiff impactors, such as stones, hail, and tools. In the case of damages by a soft impactor like birds, it is necessary to reveal the relation between the impact damage and the force applied by a soft impactor although the stiffness of the impactor could be estimated roughly from the frequency components of the sensor responses.[17] The monitoring of impact damages induced by soft impactors is a topic to be studied in a future work.

5. Conclusions

A method which monitors impact damage of FRP pressure vessels through impact force identification has been investigated in this paper. In order to obtain information on the impact that causes the damage, the impact location and force history were identified by using experimental transfer matrices which relate the impact force to the corresponding strain responses. The identified impact location was used to predict the location of the damage, while the peak value and the duration of the identified force history were used to estimate the damage initiation and the damage size, respectively. The validity of the method has been verified experimentally through the monitoring of impact damages induced by drop-weight impact tests. The knowledge obtained from the results is summarized as follows:

- By using the identification method based on experimental transfer matrices, the impact location can be identified with sufficient accuracy, regardless of the development of impact damage. Thus, the location of the damage can also be predicted accurately.
- The identified force history agreed well with the measured one when impact damages were not large. When a severe damage was induced, the peak value of the identified force history tended to be overestimated because the degradation of the structural stiffness due to the impact damage was not considered in the impact force identification. Thus, the identified peak force is not suitable for estimating the size of the damage quantitatively, but the initiation of the impact damage can be judged by comparing the identified peak force with the critical peak force. Damage size estimated from the duration of the identified force is considered to be more accurate.

References

[1] Abrate S. Impact on composite structures. Cambridge: Cambridge University Press; 1998.
[2] Staszewski WJ, Boller C, Tomlinson GR, editors. Health monitoring of aerospace structures: Smart sensor technologies and signal processing. Chichester: John Wiley & Sons; 2004.
[3] Chang CC, Sirkis J. Impact-induced damage of laminated graphite/epoxy composites monitored using embedded in-line fiber etalon optic sensors. J. Intell. Mater. Syst. Struct. 1997;8:829–841.
[4] Doyle C, Martin A, Liu T, Wu M, Hayes S, Crosby PA, Powell GR, Brooks D, Fernando GF. In-situ process and condition monitoring of advanced fibre-reinforced composite materials using optical fibre sensors. Smart Mater. Sruct. 1998;7:145–158.
[5] Takeda S, Minakuchi S, Okabe Y, Takeda N. Delamination monitoring of laminated composites subjected to low-velocity impact using small-diameter FBG sensors. Composites Part A. 2005;36:903–908.
[6] Minakuchi S, Okabe Y, Mizutani T, Takeda N. Barely visible impact damage detection for composite sandwich structures by optical-fiber-based distributed strain measurement. Smart Mater. Struct. 2009;18:085018.
[7] Minakuchi S, Takeda N, Takeda S, Nagao Y, Franceschetti A, Liu X. Life cycle monitoring of large-scale CFRP VARTM structure by fiber-optic-based distributed sensing. Composites Part A. 2011;42:669–676.
[8] Takeda S, Aoki Y, Nagao Y. Damage monitoring of CFRP stiffened panels under compressive load using FBG sensors. Compos. Struct. 2012;94:813–819.
[9] Todoroki A, Yanaka Y, Shimamura Y. Delamination monitoring of graphite/epoxy laminated composite plate of electric resistance change method. Compos. Sci. Tech. 2002;62:1151–1160.
[10] Swait TJ, Jones FR, Hayes SA. A practical structural health monitoring system for carbon fibre reinforced composite based on electrical resistance. Compos. Sci. Tech. 2012;72: 1515–1523.
[11] Sung DU, Oh JH, Kim CG, Hong CS. Impact monitoring of smart composite laminates using neural network and wavelet analysis. J. Intell. Mater. Syst. Struct. 2000;11:180–190.
[12] Jang BW, Park SO, Lee YG, Kim CG, Park CY. Detection of impact damage in composite structures using high speed FBG interrogator. Adv. Compos. Mater. 2012;21:24–44.
[13] Hu N, Matsumoto S, Nishi R, Fukunaga H. Identification of impact forces on composite structures using an inverse approach. Struct. Eng. Mech. 2007;27:409–424.
[14] Fukunaga H, Hu N. Damage monitoring of CFRP structures based on impact force identification. In: Asia-Pacific Workshop Struct. Health Monit. Proceedings; 2006 Dec 4–6; Yokohama (Jpn): Keio University; 2006.
[15] Fukunaga H, Miura Y, Tajima M, Hu N. Impact damage monitoring of composite structures based on impact force identification. In: Takeda N, Pipes RB, Gillespie J, editors. US-Japan Conf. Compos. Mater. 2008. Proceedings; 2008 Jun 67; Tokyo (Jpn): Nihon University; 2008.
[16] Abrate S, editor. Impact engineering of composite structures. Springer: Wien; 2011.
[17] Umino T, Miura Y, Sugimoto S, Kameyama M, Hu N, Fukunaga H. Experimental impact force identification of CFRP stiffened panel under multiple loading. J. Jpn. Soc. Compos. Mater. 2009;35:106–111. Japanese.